Graphical Models 95 (2018) 29–41

Contents lists available at ScienceDirect

Graphical Models

journal homepage: www.elsevier.com/locate/gmod

Large-eddy simulations of pedestrian-level ventilation for assessing a satellite-based approach to urban geometry generation

Weiwen Wang[a,*], Yong Xu[b], Edward Ng[a,b,c]

[a] School of Architecture, The Chinese University of Hong Kong, Hong Kong Special Administrative Region
[b] Institute of Future Cities, The Chinese University of Hong Kong, Hong Kong Special Administrative Region
[c] Institute of Environment, Energy, and Sustainability, The Chinese University of Hong Kong, Hong Kong Special Administrative Region

ARTICLE INFO

Article history:
Received 20 January 2017
Revised 7 June 2017
Accepted 13 June 2017
Available online 15 June 2017

Keywords:
Large-eddy simulation
Pedestrian-level ventilation
Building height retrieval
Building footprint
Hong Kong

ABSTRACT

Realistic digital elevations of urban areas are required in urban studies but are not always available. There is a need to extract urban information from satellite images that can be used for, but not limited to, studies of the urban wind environment. This study evaluates urban geometries, including building heights and building footprints, extracted from various satellite images by large-eddy simulations for air ventilation assessment (AVA). The result shows that building heights extracted from TerraSAR-X synthetic aperture radar (SAR) images and the fused results of SAR and WorldView-2 optical (stereo) images are suitable for AVA. Better performance in representing tall buildings, rather than low buildings, is found to be more important for AVA purposes. Moreover, the performance of building geometries retrieved from fused satellite images with and without real building footprints is comparable, which suggests that building footprints extracted from stereo images are reliable.

1. Introduction

Wind comfort and wind safety for pedestrians are important requirements for city design and urban planning [1]. In subtropical high-density cities such as Hong Kong, urbanization causes a number of problems such as urban heat islands and air pollution [2]. Urban ventilation is found to be a way of mitigating these problems [3–5]. Good air ventilation is very important for high-quality healthy living and comfortable thermal sensations. Thermal comfort can be achieved by capturing natural wind. To achieve neutral thermal sensation in an urban environment, a wind speed of 0.9–1.3 m/s is needed for a person wearing light clothing under shaded conditions [6]. However, a distinction should be made between ventilation for air quality and ventilation for thermal comfort. When the purpose is to study ventilation for air quality, the main parameters are flow rate and turbulent transport at rooftop level, which provide dilution capacity for contaminants and remove contaminants from street canyons. When the purpose is to study ventilation for thermal comfort, the main parameter is wind velocity at the pedestrian level. This study focuses on ventilation for thermal comfort, so the main parameter to be investigated is the wind velocity ratio at the pedestrian level.

In the literature of urban air ventilation, various research methods have been used to describe the complex flows over urban environments. Computational fluid dynamics (CFD) techniques such as the Reynolds-averaged Navier–Stokes (RANS) model, large-eddy simulation (LES), and direct numerical simulation (DNS) are among the commonly used tools [7,8]. Urban ventilation is strongly influenced by wind speed and direction, which in turn are affected by three-dimensional urban morphology [9–11]. Unfortunately, realistic digital elevations of urban areas required in CFD studies are not always available for open access, especially in the less developed regions of the world where urban population growth is concentrated. There is a well-known problem of urban data quality and availability in these regions. Furthermore, surface geometries and urban morphologies are found to have a significant influence on urban heat islands [12], especially for regions with a hot and humid microclimate [13]. High-resolution digital elevations have been extensively used in studies of urban climate and outdoor thermal comfort [14]. Therefore, there is a need to develop methodologies of extracting urban geometries in urban areas that can be used for, but not limited to, studies of urban ventilation.

The term ‘urban geometry’ in this study reflects the physical characteristics of an urban form, simply referring to building footprints and building heights. Field measurement and satellite-based data are available methods for obtaining urban information. Classical field measurement is highly accurate for small study areas but is time-consuming. Satellite technology provides a fast

* Corresponding author.
E-mail address: w.wang@cuhk.edu.hk (W. Wang).

http://dx.doi.org/10.1016/j.gmod.2017.06.003
1524-0703/

and economic way to obtain large-area morphological information. There are three kinds of remote sensing technologies that can extract building information: stereo photogrammetry technology with pairs of optical images (hereafter referred to as stereo images), synthetic aperture radar (SAR) technology, and light detection and ranging data (LiDAR) technology. However, there are limitations to these methods: (1) stereo images tend to underestimate the height of tall buildings, and taller buildings produce larger errors [15]; (2) the interferometry of SAR provides noisy and incomplete data, particularly for high-density urban areas where the mutual interference of surrounding buildings is significant [16,17]; and (3) LiDAR data are expensive and are limited by flight restrictions for applications in large urban areas [18]. Therefore, recent studies have also been devoted to the integrated use of different kinds of data for building data retrieval [17,18].

The objective of the present study is to assess the performance of building geometry extractions from different kinds of satellite images for potential use in urban ventilation studies with CFD techniques. Evaluation of building data extraction from satellite images from the perspective of a particular application, i.e., urban ventilation, has rarely been attempted to date as far as we know. What affects pedestrian comfort directly is the wind flow within cities, in particular, the local turbulence level [7]. We therefore use an LES model to produce CFD simulations in this study. LES overcomes the deficiencies of RANS by explicitly resolving large, energy-containing turbulent eddies and parameterizing only small (subgrid) scale turbulence [19,20]. The dimensionality, spatial resolution, and turbulence intensity that an LES model can handle are superior compared to most of the other methodologies, and sometimes also to other CFD models, i.e., RANS and DNS [21]. LES provides not only mean flow fields but also instantaneous turbulences, which are especially important for human comfort at the pedestrian level in the urban canopy layer [22].

To make the paper easier to follow, we clarify here the goals of each section and the main conclusions before going into detail: neighborhood-scale urban geometries are introduced in Section 2, including the actual (measured) data and those extracted from satellite images for assessment. In Section 3, we introduce the LES model used in this study, including the definition of the pedestrian-level ventilation indicator, velocity ratio, and basic model setups in Section 3.1, and LES model validation by CFD guidelines in Section 3.2. Details of the main results are presented in Sections 4 and 5. Section 4 evaluates building height extraction with actual building footprints. This section concludes that building heights extracted from SAR images and the fused results of SAR and stereo images are suitable for air ventilation assessment (AVA) studies, and better performance in representing tall buildings, rather than low buildings, is found to be more important for AVA purposes. Section 5 evaluates building footprints retrieved from stereo images and concludes that such a method is reliable. Sections 6 and 7 further discuss and summarize the study.

2. Neighborhood-scale urban geometries

Hong Kong is one of the most densely built cities in the world. It is located in the Pearl River Delta region of China, which is experiencing rapid urbanization. The Mong Kok area on the Kowloon Peninsula of Hong Kong has tall buildings and narrow streets that form deep street canyons. Irregular street orientations and building layouts make the urban morphology in the region more complex. Mong Kok is herein chosen as the case study for this paper.

In a recent study, we proposed an approach that jointly uses high-resolution WorldView-2 stereo images and multi-temporal TerraSAR-X SAR images to retrieve urban geometries in high-density urban areas, which has the advantage of both datasets [23]. Procedures of the proposed approach are shown in Fig. 1a. In the first step of the present study, actual (measured) urban geometries in a neighborhood of Mong Kok provided by the Hong Kong Planning Department are utilized as topography input for the LES model. The domain is 1.2 km × 1.2 km, as given in Fig. 2a. The data have a horizontal resolution of 2 m. The methodology proposed in Fig. 1a for retrieving building heights in urban areas using both stereo and SAR images assumes that the building footprints are known and involves two main stages: First, estimated initial building heights are retrieved from stereo and SAR images, respectively; second, according to an object-based fusion approach, the initial building heights are then combined. The bias of building heights between actual data and data extracted from stereo images, SAR images, and the fused result of the two kinds of images is given in Fig. 2b, c, and d, respectively. The four sets of data in Fig. 2 are topography inputs for simulation of ventilation in the first step of building data assessment.

However, in reality, building footprints are generally unknown if building heights are unknown. Therefore, urban geometries including both building footprints and building heights are extracted from satellite images, as shown in Fig. 1b. The method in Fig. 1b is similar to that in Fig. 1a except that the building footprints are extracted from stereo images rather than being provided by measurements. Building footprints are retrieved only from stereo images, as these are pairs of optical images and have small positioning error. The performance of these building data in terms of pedestrian-level ventilation in large-eddy simulations is evaluated in the second step of this study. In this step, we utilize a 2 km × 2 km neighborhood in Mong Kok, with a horizontal resolution of 2 m. Three sets of data will be involved: actual (measured) data, the fused result of both kinds of satellite images (stereo and SAR) with real building footprints, and the fused result with building footprints extracted from stereo images. These three sets of data will be shown together with the simulated velocity ratios in a later section.

3. The parallelized large-eddy simulation model

The LES model used in this study is the Parallelized LES Model (PALM), which was developed at the Institute of Meteorology and Climatology of the Leibniz Universität Hannover in 1997 [24]. PALM has been validated for simulating flows and turbulence characteristics at the street-canyon and neighborhood scale and has been widely used in studies of urban street-canyon flows in recent years [25–29], including high-density urban areas in Hong Kong [30] and Macau [22]. The code used in this study is the most updated PALM version 4.0 [31]. More details can be found on the PALM homepage (https://palm.muk.uni-hannover.de/trac).

3.1. Indicator and simulation setup

In AVA studies, we are especially interested in pedestrian-level wind velocity. The wind velocity ratio (VR) is used as an indicator, which is calculated by

$$VR = V_p / V_\infty, \quad (1)$$

where V_P is the wind velocity at the pedestrian level (2 m above the ground), and V_∞ is the wind velocity at the top of the wind boundary layer and is not affected by ground roughness [4]. A top boundary layer of 500 m is commonly used in Hong Kong AVA studies [32].

Model domain and grid spacing: in the main runs of Section 4 (evaluation of building height extraction with actual building footprints), the model domain, i.e., the input building data size, is 1.2 km by 1.2 km. In Section 5 (evaluation of building footprints retrieved from stereo images), the model domain is 2 km by 2 km. In both Sections 4 and 5, horizontal grid spacing sizes are

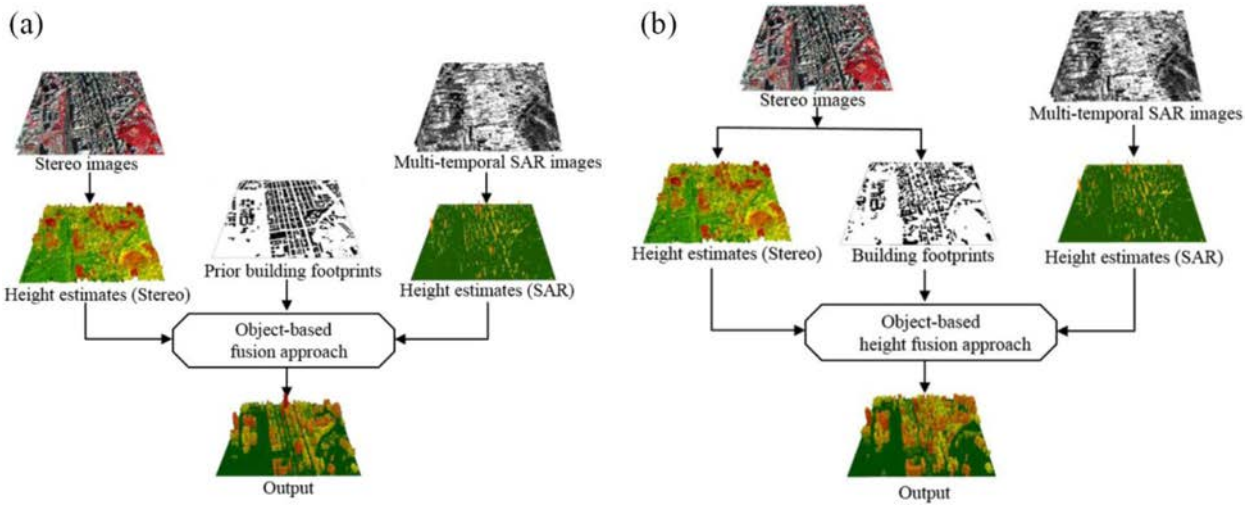

Fig. 1. Procedure of the satellite-based approach for urban geometry retrieval: (a) Building footprints provided by measurements, and (b) building footprints extracted from stereo images.

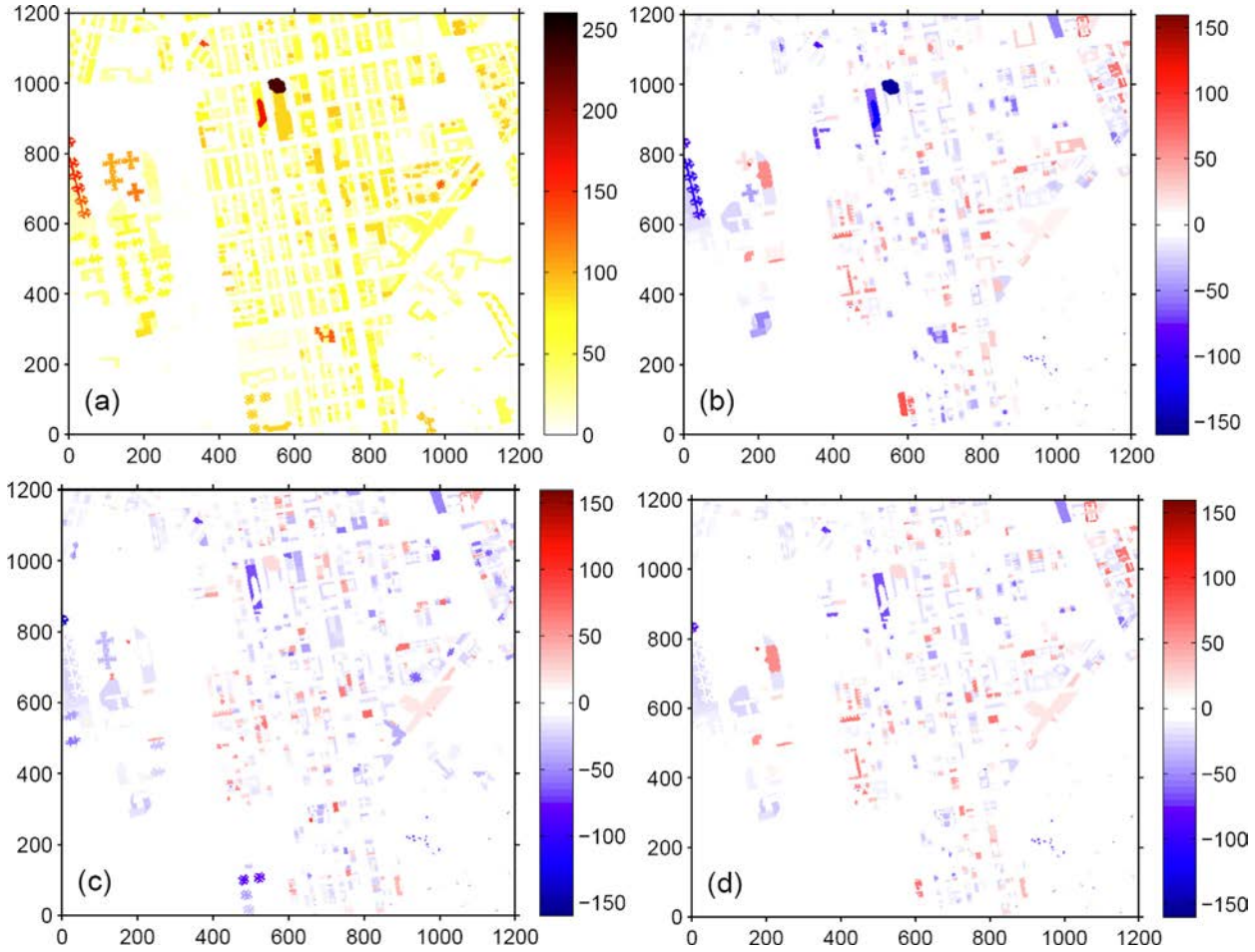

Fig. 2. (a) Actual urban elevations (building heights) in a 1.2 km × 1.2 km neighborhood in Mong Kok. Bias between actual data and data extracted from (b) stereo images, (c) SAR images, and (d) the fused result of the two kinds of images.

equidistantly 2 m. The vertical grid spacing is 2 m below 300 m and stretched with a stretch factor of 1.08 above, as the tallest building on-site is below 300 m. In PALM, scalar variables are defined at the grid centers, while velocity components are shifted by half of the grid spacing. Therefore, horizontal wind velocity output from the 1 m and 3 m levels is linearly interpolated (averaged) to obtain V_P at 2 m above the ground. V_∞ is derived from 500 m.

Input wind, time step length, and simulation time: as we are focusing mainly on the velocity ratio, the input wind speed is not very important, and if high wind speed is used, more computational time will be needed because the time step has to be shorter.

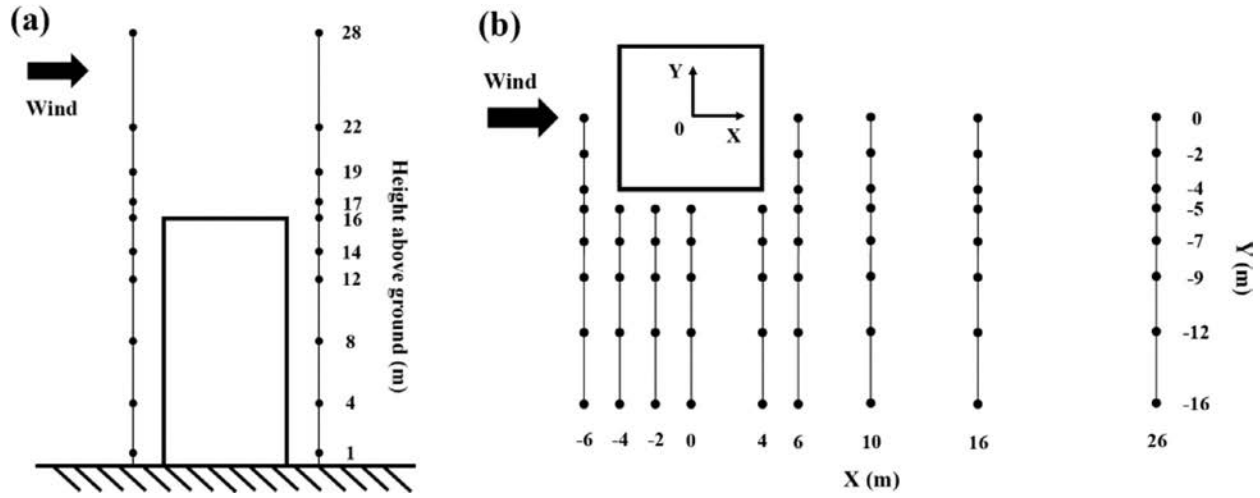

Fig. 3. Locations of test points in the Architectural Institute of Japan (AIJ) guidelines setup for a single building: (a) Lateral view of the two profiles and 20 test points taken at 2 m away from the building to windward and leeward. (b) Aerial view of 60 horizontal test points around the building at 1 m above the ground. This figure is adopted and modified from the AIJ guidelines (http://www.aij.or.jp/jpn/publish/cfdguide/index_e.htm).

Therefore, a low-velocity wind of 1.5 m/s is prescribed to save computational time. The time step lengths are optimized in PALM. The total simulation time is 6 h. The first 4 h are excluded in the analysis of the results, as the turbulences need this time to spin-up. The simulated results from the 5th to the 6th h are averaged for analysis. East (90°) and southwest (225°) winds, the prevailing annual and summer winds in Hong Kong, respectively, are simulated.

Boundary conditions: the simulations are restricted to neutral atmospheric stratification, which means that only winds are prescribed; thermal effects are not considered. Calculation of the temperature equation is switched off. The no-slip bottom boundary condition and the free-slip top boundary condition are applied to the horizontal velocity components. As the targeted area is surrounded by urban areas, a simple cyclic (periodic) boundary condition setup in both the streamwise and spanwise directions is sufficient for the task.

3.2. Model validation

We use the CFD guidelines proposed by a working group from the Architectural Institute of Japan (AIJ) to verify the PALM codes. The AIJ guidelines are based on the results of cross-comparisons of CFD predictions, wind tunnel tests, and field measurements [33]. The validation of PALM using AIJ guidelines is the same as that employed by a previous study [34], from which the following text is derived with minor modifications.

We conducted LES experiments with the 2:1:1 shape building model as well as simple building blocks that comply with AIJ guidelines. The CFD setups and experimental data for verification can be found on the AIJ website (www.aij.or.jp/jpn/publish/cfdguide/index_e.htm). Details for the single-building case can be found in Mochida et al. [35], while introductions of all seven test cases can be found in Tominaga et al. [33].

For the single-building case, the horizontal computational domain size is 172 m × 108 m. An equidistant horizontal grid size of 0.5 m is used. In the vertical direction, a grid size of 0.5 m is adopted below 24 m and a stretch with a stretch factor of 1.05 is applied above. With 90 vertical levels, the domain height is about 100 m. The building height is 16 m. It is noteworthy that for this simulation of a single building, a noncyclic boundary condition in the streamwise direction is adopted. Otherwise, it will become a simulation of an infinite row of buildings. Validation is accomplished by comparing PALM-computed results and AIJ guidelines in terms of wind profiles around the building and wind velocity taken from near-surface test points. Fig. 3a shows the profiles at 2 m away from the single building to windward and leeward, while Fig. 3b shows the locations of 60 test points at 1 m above the ground.

The inlet mean wind profile in the PALM experiment is the same as that given in the guidelines, as shown in the black profile in Fig. 4a. Fig. 4a compares velocity profiles at 2 m away from the single building to windward (red lines) and leeward (blue lines). Dashed lines represent AIJ referential data, while solid lines indicate results predicted by PALM. Stronger rooftop vortex and velocity fluctuation compared to AIJ data can be observed in Fig. 4a, but overall good agreement between the two suggests that PALM can capture the wind profile features around the building. As this study focuses on pedestrian-level ventilation, the computational performance of PALM in reproducing near-surface velocity may be more important. Fig. 4b is a scatter plot of PALM-computed velocity and AIJ experimental data at 60 test points. The comparison in Fig. 4b gives substantial confidence to using PALM in the study of pedestrian-level wind flow, as all points are located close to the diagonal line. A linear regression with an R^2 of 0.9 can be obtained.

Validation for the simulation of air flow around only a single building may not be convincing for this study. For validation cases with simple building blocks, the building arrays, inlet mean wind profile, and locations of test points are shown in Fig. 5. The experiments include 9 buildings with a uniform building height of H = 20 m, except the one in the middle, which is prescribed a varying building height for each case of 0H, 1H, and 2H, respectively (Fig. 5a). The buildings are horizontally foursquare and both the buildings and the streets are 20 m wide. In the PALM experiments, the computational domain size is 300 m × 200 m × 120 m. An equidistant grid size of 0.5 m is used both horizontally and vertically. The inlet mean wind profile is the same as that given in the guidelines and shown in Fig. 5b. Velocity values taken from 120 test points at 2 m above the ground are used to validate the PALM simulation. The test point locations are shown in Fig. 5c (black dots).

The validation results are shown in Fig. 6. Generally, the scatter dots are located close to the diagonal lines, but the results predicted by PALM may have slightly underestimated the near-surface velocity compared to AIJ guidelines, particularly in those test points with relatively low wind speed. A linear regression with an R^2 of 0.82, 0.77, and 0.60 can be obtained for cases 0H, 1H, and 2H, respectively. The complex level of the building arrays may affect the accuracy of the PALM prediction. But in general, no sig-

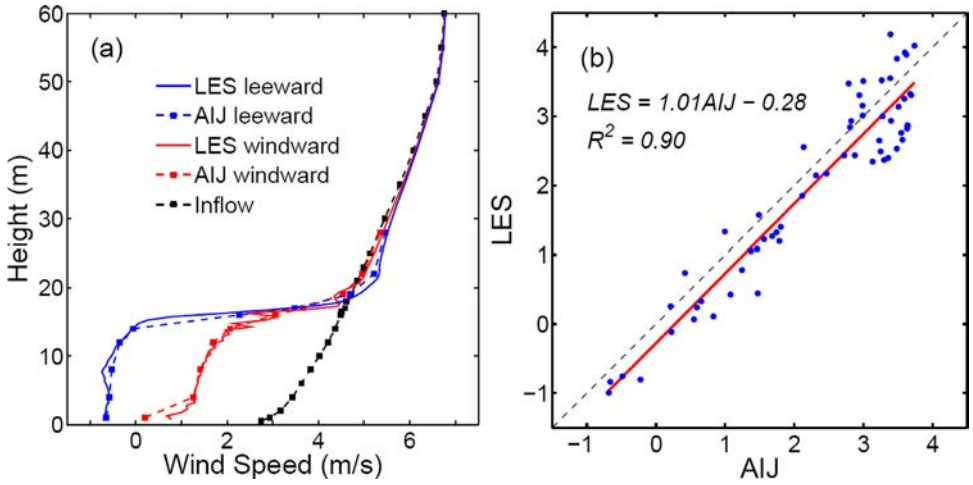

Fig. 4. Cross-comparison between Architectural Institute of Japan (AIJ) experimental data and PALM results: (a) Vertical wind profiles in the windward (red lines) and leeward (blue lines) position at 2 m from the building; the inflow is shown by the black profile. (b) Linear regression between AIJ and PALM results in the test points at 1 m above the ground. (For interpretation of the references to colour in this figure legend, the reader is referred to the web version of this article.)

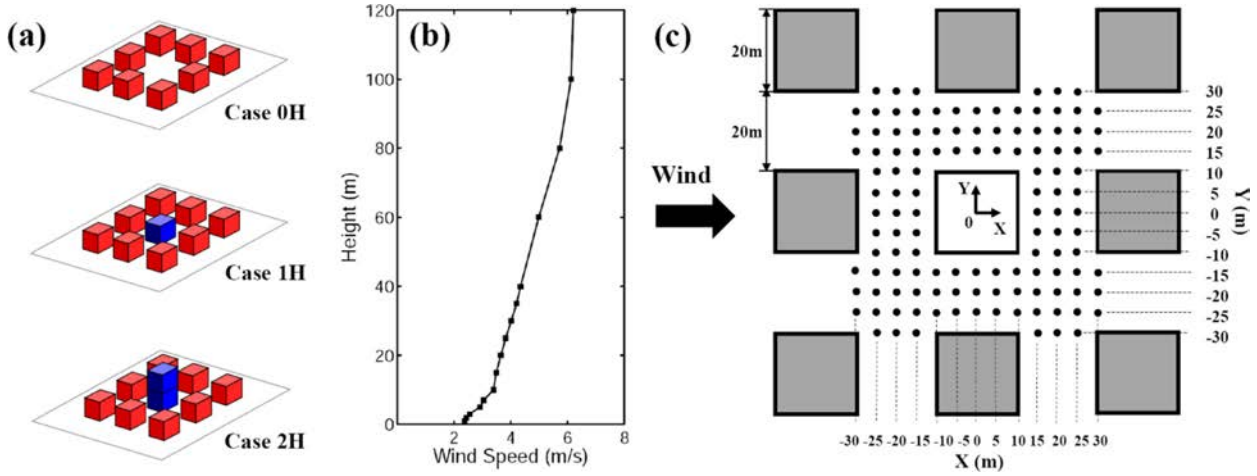

Fig. 5. Setups of validation cases for simple building blocks: (a) Building arrays of three cases, (b) The inlet mean wind profile, and (c) Building geometries (boxes) and locations of test points (black dots). This figure is adopted and modified from the AIJ guidelines (http://www.aij.or.jp/jpn/publish/cfdguide/index_e.htm).

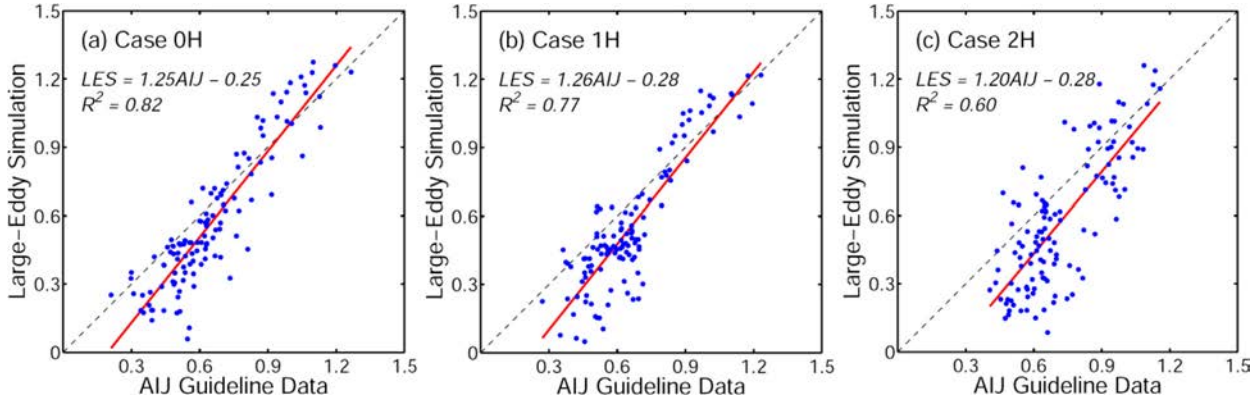

Fig. 6. Linear regression between referential velocity of Architectural Institute of Japan (AIJ) guidelines and large-eddy simulation (LES) results taken from 120 test points at 2 m above the ground in simple building blocks for (a) Case 0H, (b) Case 1H, and (c) Case 2H.

nificant deviations are found in the above validations. The PALM model is therefore deemed to be a suitable LES tool for this study.

4. Building height extraction with real footprints

This section compares building information extracted from stereo images, SAR images, and the fused results of both types of images to the actual data. As building footprints are provided by measurements (Fig. 1a), the major parameter to be retrieved and evaluated from satellite images is building height. With four sets of topography data (Fig. 2) and two input wind directions, results from eight PALM experiments are described below.

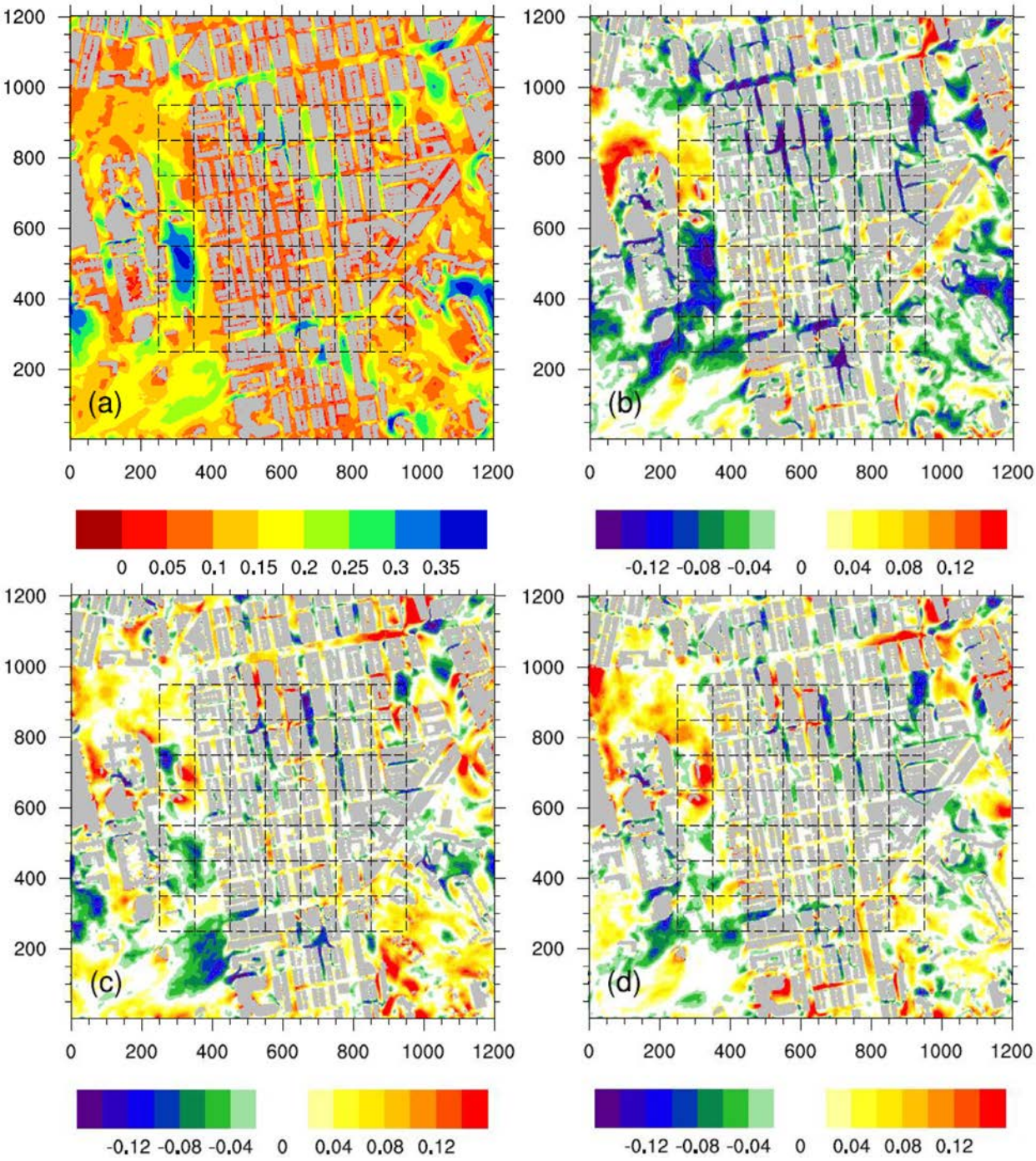

Fig. 7. (a) PALM-computed velocity ratio in actual topography; deviations of VR from actual topography and topography retrieved from (b) stereo images, (c) SAR images, and (d) fused result of the two images. The dashed black boxes denote the 100 m × 100 m domains for the zonally averaged velocity ratio. Wind input is from the east (right).

4.1. Effects of average size

Results of the PALM-computed velocity ratio with wind input from the east (southwest) with actual topography and biases from retrieved urban geometries are given in Fig. 7 (Fig. 8). These simulated results in urban data retrieved from satellite images are evaluated first in terms of area-averaged velocity ratios. We select two kinds of grid sizes to check whether the comparative results are sensitive to the average size. One is 100 m × 100 m while the other is 50 m × 50 m, with a unique buffer width of 250 m. A buffer width of 250 m can match the requirement of AVA [4], as the tallest building in the research area is 255 m (Fig. 2). Generally, it is suggested that simulated results in the outer regions near the horizontal boundary are not reliable. The 100 m × 100 m grids are shown in dashed boxes in Figs. 7 and 8. For the grid size of 50 m × 50 m, the resolution is simply doubled.

Table 1 lists all the root mean square errors (RMSEs) of PALM-calculated velocity ratios between extracted and actual topography. The largest value in each row is in bold, and the smallest value is underlined. Referring to the average size, the results can be compared for wind input from the east and southwest, respectively. It is found that the average sizes do not change the order of RMSEs from the three sets of topography in the case of southwest wind. The average size has a slight effect on the RMSE order in the case

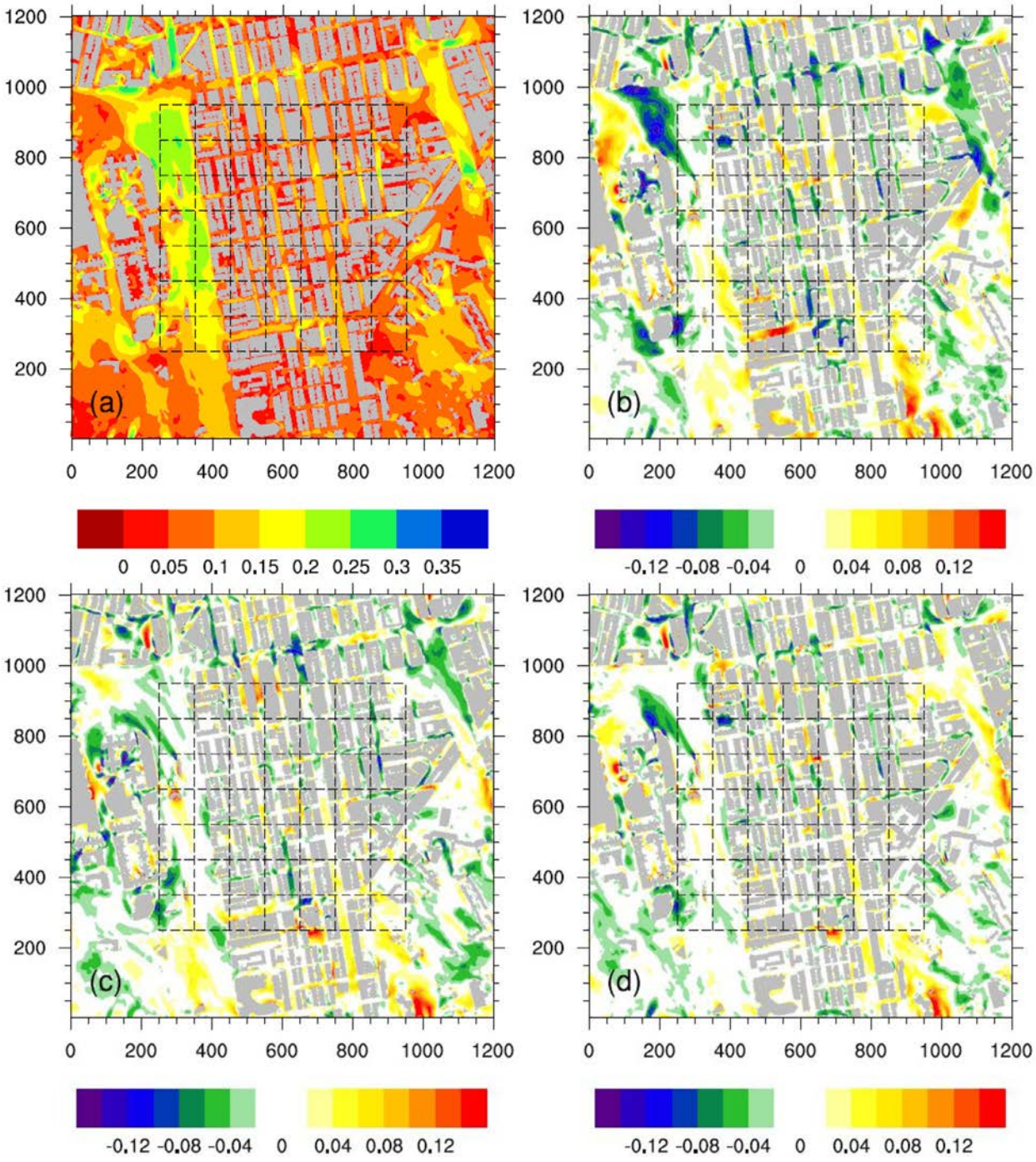

Fig. 8. Same as Fig. 4 but with wind input from the southwest.

Table 1
Root mean square errors (RMSEs) of velocity ratios between retrieved and actual building heights in different LES experiments (wind directions) and average sizes. The largest (smallest) value in each row is in bold (underlined).

Wind direction	Average size	RMSEs stereo	RMSEs SAR	RMSEs fused
East	100 m × 100 m	**0.040**	0.026	0.028
East	50 m × 50 m	**0.046**	0.035	0.035
Southwest	100 m × 100 m	**0.017**	0.014	0.009
Southwest	50 m × 50 m	**0.023**	0.020	0.016

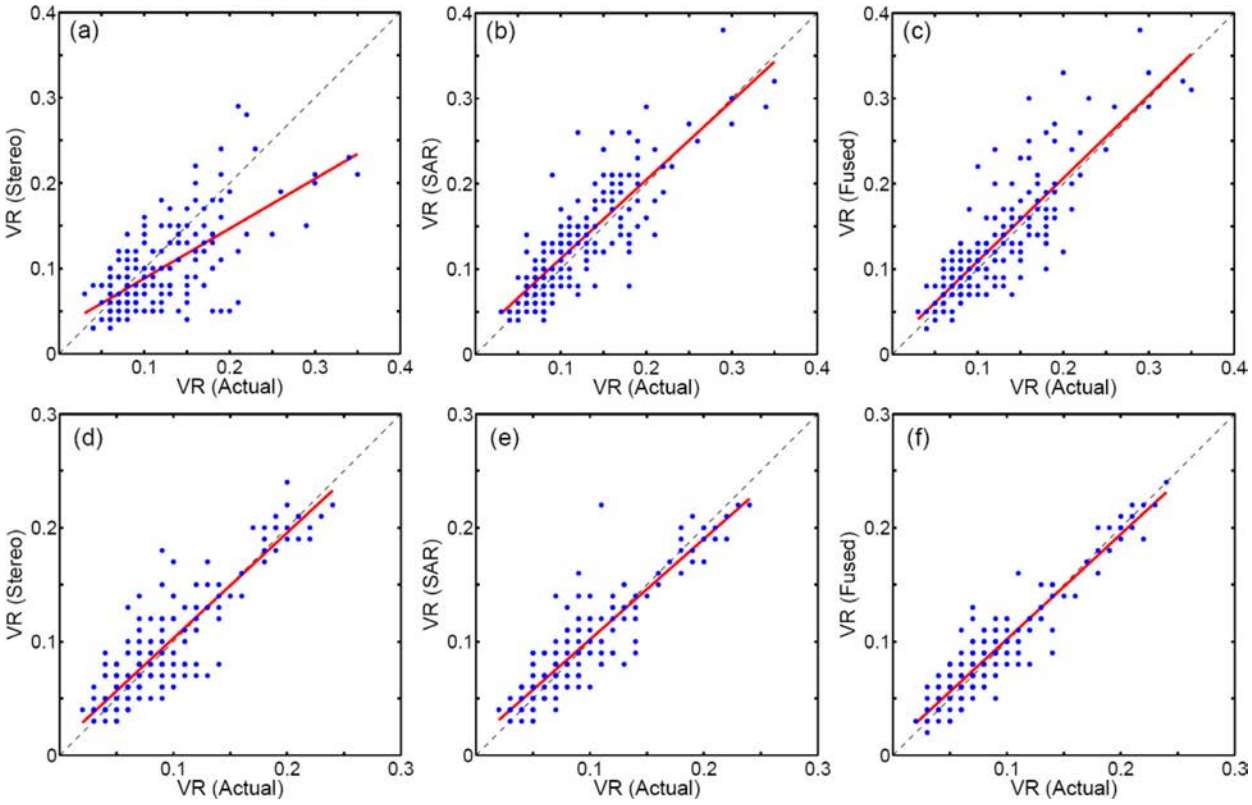

Fig. 9. Scatter plots (blue dots) and linear regressions (solid red lines) of PALM-computed velocity ratios with actual topography and topography extracted from (a, d) stereo images, (b, e) SAR images, and (c, f) fused result of the two images. Wind input is from the east (southwest) for a–c (d–f). Average size is 50 m × 50 m. (For interpretation of the references to colour in this figure legend, the reader is referred to the web version of this article.)

of east wind, as can be seen from Table 1. Generally, the effects of average size on the overall RMSEs are not significant.

4.2. Effects of wind direction

Generally speaking, changes in the input wind direction cause modifications in local (subdomains in the neighborhood site) urban morphology and geometry parameters in AVA, such as the frontal area index. The local roughness length in the LES model takes effect when the wind sweeps across the ground and walls. The higher the proportion of ground and walls the wind has to sweep across, the larger the friction effects on the wind. Therefore, effects of wind direction on air ventilation are combined with local roughness length. RMSEs in Table 1 suggest that building heights extracted from stereo images give the worst performance compared with the other two methods. When comparing SAR and fused results, it is found that the fused results have better performance with a southwest wind, while the SAR result is slightly better with an east wind.

Fig. 9 further demonstrates the performance of data retrieved using different methods. As Section 4.1 pointed out that the result is not sensitive to the average size (50 m × 50 m or 100 m × 100 m), the scatter plots and linear regressions in Fig. 9 are made with samples from the average size of 50 m × 50 m, which yields more samples than the average size of 100 m × 100 m. It can be seen that the stereo result has a large bias from the actual topography in the LES experiment with east wind (Fig. 9a), while it has a better performance in the LES experiment with southwest wind (Fig. 9d). The performances of SAR and the fused results are close to each other and reasonable in the LES experiment with both east and southwest wind (Figs. 9b, c, e, and f).

Beyond taking averaged values of velocity ratios in domains, say 50 m × 50 m or 100 m × 100 m, to statistically capture the spatial differences in the velocity ratios given in Figs. 7 and 8, the distributions of these ratios taken from random test points are shown in Fig. 10. In this analytical procedure, all street (non-built) grid points inside the assessment area (250 m away from the lateral boundary in two horizontal directions, as shown in the dashed boxes in Figs. 7 and 8) in each scenario are stored in a 1-D array, and 1000 test points are randomly taken from each array. The random function calculates the interval between test points using a normal distribution with a mean of the array size divided by the number of test points (1000) and a standard deviation of 25% of the mean; thus, the test points are randomly spread throughout the whole assessment area. Furthermore, sensitivity tests were conducted regarding the number of test points, and no significant differences were found when the number of test points was larger than 200, which means that any sample number above 200 would be enough to produce the distributions in Fig. 10.

Fig. 10 shows that for east wind input, the distribution of velocity ratios taken from random test points of the SAR and fused results are comparable to that of the actual case, while the stereo results obviously overestimate the probability of low velocity ratios around 0.05. For southwest wind input, all three satellite-based results are comparable to the actual case. This is consistent with the area-averaged result shown in Fig. 9.

4.3. Effects of building height biases

Using the average absolute difference from measured data to evaluate the retrieved results, Xu et al. (2015) [23] discovered that stereo images provide better results for buildings below 100 m, particularly for buildings below 50 m, while SAR images provide

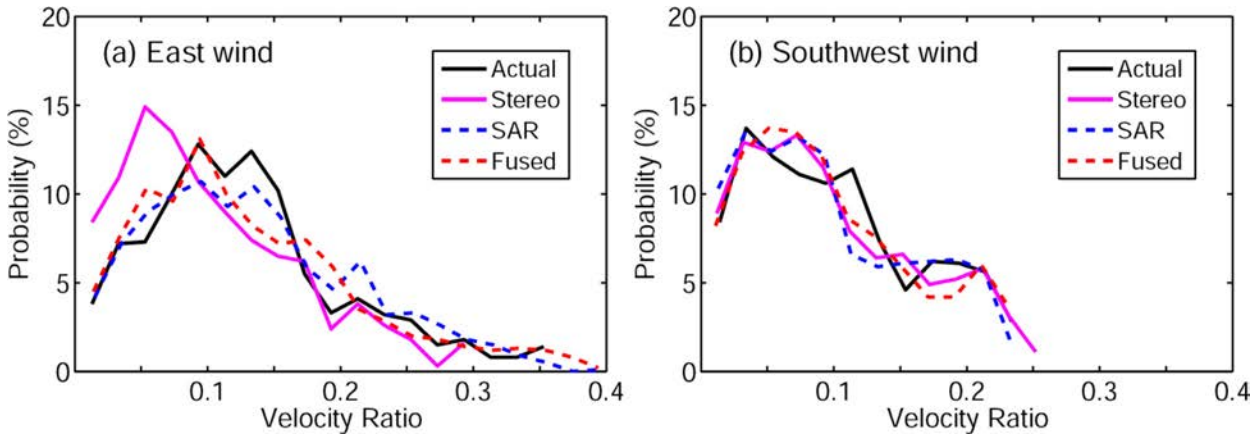

Fig. 10. Distributions of velocity ratios referenced at 2 m above the ground taken from random test points.

better results for higher buildings (e.g., above 100 m). Tall buildings are underestimated by the stereo images, which can be seen in Fig. 2b. If we check the details of VR bias inside the congested urban spaces (dashed grid boxes in Figs. 7 and 8), which are reliable because lateral boundary areas are avoided, it can be seen that a larger bias can be found in the stereo result than in the SAR result in the simulations, particularly for wind input from the east. This implies that a better representation of higher buildings may contribute more to the quality of pedestrian-level ventilation simulations, as high-rise buildings can experience high wind loads and concentrate pedestrian-level winds [36,37].

We further demonstrate this dynamically using an extreme case: the tallest building is at a coordinate of approximately $x = 550$ m, $y = 1000$ m (Fig. 2). Fig. 11 shows the vertical velocity of the x–z cross section at $y = 1000$ m, which crosses the tallest building on the site. The results of the LES experiment with east wind input from all four topography datasets are shown. It is obvious that both the SAR and fused results can capture the high-rise building as well as the vertical motion around it, while the stereo result fails to do so. When the wind comes from the east (right-hand side of Fig. 11), the high-rise building blocks the wind and results in strong sinking motion on its windward side and rising motion in front of its steeple and on the leeward side. This vertical motion will further induce horizontal winds and gusts at the pedestrian level and hence increase ventilation in the subdomain where the high-rise building stands. It is also noteworthy that a similar structure of vertical motion can be found around relatively high buildings in Fig. 11, which suggests that better performance in representing higher buildings, rather than lower buildings, is more important in building height extraction for AVA purposes.

5. Comparison of fused results with real and extracted footprints

In this section, we evaluate building geometries retrieved by the satellite-based method proposed in Fig. 1 by comparing their PALM-computed velocity ratios to the actual ones. We have two sets of retrieved data to be assessed. In one, proposed by Fig. 1a, building footprints are provided by measurements, and in the other, proposed by Fig. 1b, building footprints are extracted from stereo images. Building heights in both sets of data are the fused results of stereo and SAR images. The three sets of urban morphologies and PALM-computed velocity ratios of six experiments are shown in Fig. 12. For area-averaged velocity ratio, we again select two kinds of grid sizes to check whether the comparative results are sensitive to the average size. One is 200 m × 200 m while the other is 100 m × 100 m, with a unique buffer width of 300 m. The simulated results in the outer regions near the horizontal boundary are probably not reliable. The 200 m × 200 m grids are shown in dashed boxes in Fig. 12. For the grid size of 100 m × 100 m, the resolution is simply doubled.

The RMSEs of PALM-computed velocity ratios between extracted and actual topography are compared in Table 2. To evaluate the performance of building geometries extracted from fused satellite images with and without real building footprints, the larger RMSE value in each row is in bold. Referring to the average size, the results can be compared for wind input from the east and southwest, respectively. The average sizes do not change the order of RMSEs from the two sets of topography in either input wind direction. The effects of average size on the overall RMSEs are not significant. Consequently, the scatter plots and linear regressions in Fig. 13 are made with samples from the average size of 100 m × 100 m, which yields more samples than the average size of 200 m × 200 m.

Table 2 and Fig. 13 suggest that building geometries retrieved from fused satellite images with and without real building footprints are both acceptable in the LES experiments with southwest wind input, given their small RMSE values and well-fitted linear regression. Moreover, the performance of building data retrieved with real building footprints is slightly better than that of building footprints extracted from stereo images. However, the results for LES experiments with east wind input for both cases are not so convincing, as can be seen in Figs. 13a and b. The RMSEs are large compared to those of the southwest wind experiments (Table 2). In these cases, the RMSEs of real footprint data are larger than those of the extracted footprint data, but they are very close.

Fig. 14 shows the distributions of velocity ratios taken from 1000 random test points in the assessment area of Fig. 12. This further demonstrates the findings of Table 2 and Fig. 13 that, in the case of southwest wind, fused results are comparable to those of the actual case both with and without real building footprints, while in the case of east wind, the results are not so convincing, as both retrievals underestimate the probability of a velocity ratio below 0.1.

6. Discussion

Extraction of urban information from satellite images has become a hot topic in remote sensing studies, as these techniques are important for urban studies [38]. Therefore, assessment of these techniques should be done in combination with urban applications, which is the origin of the present study. As a case study, building information in a high-density urban area in Mong Kok, Hong Kong, including both actual information and that retrieved from satellite images, is adopted from a newly published report [23] and is evaluated by comparing pedestrian-level ventilation in an LES

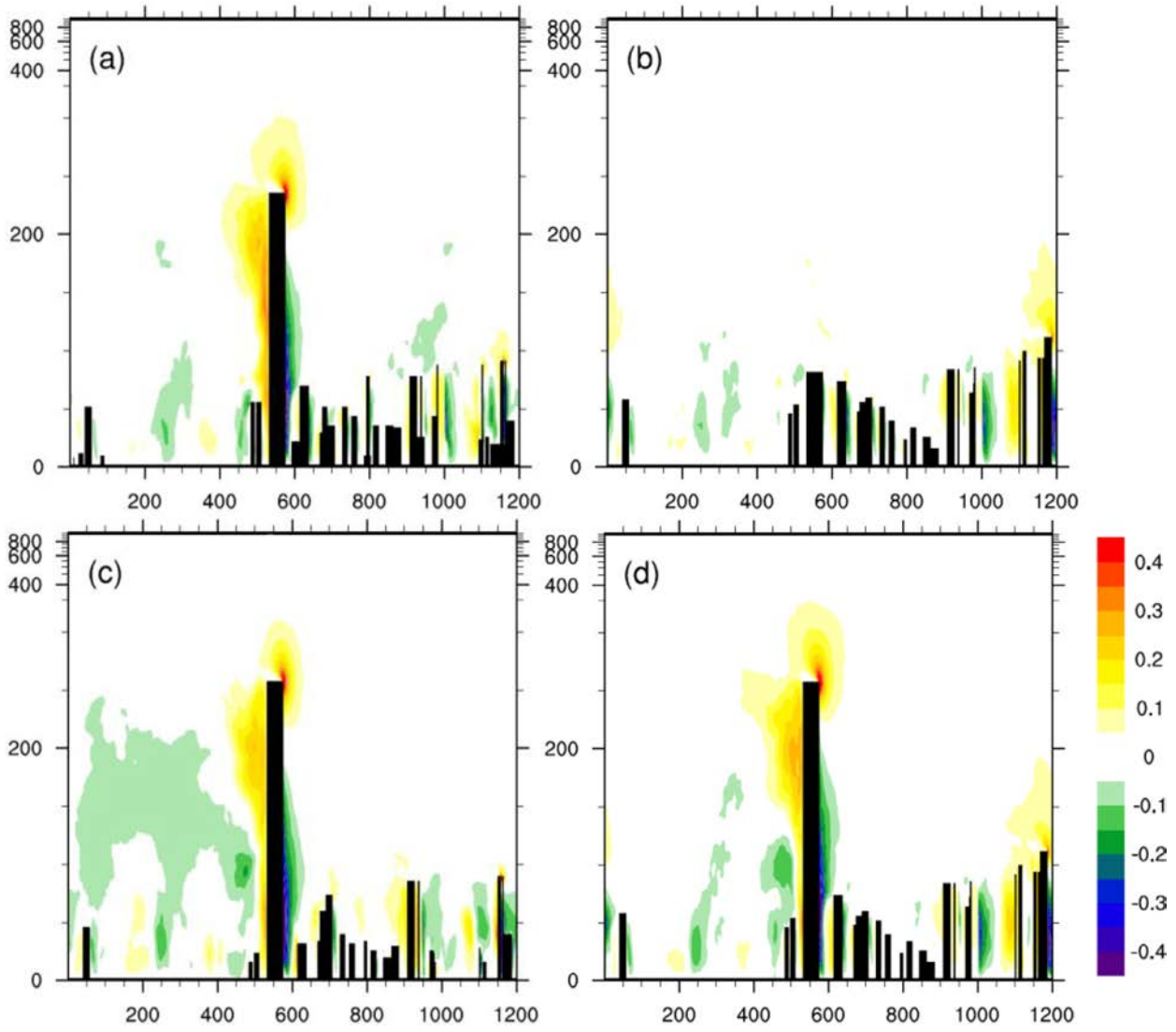

Fig. 11. Time-averaged vertical velocity in a specific section with a high-rise building from (a) actual urban elevations, and urban elevations extracted from (b) stereo images, (c) SAR images, and (d) fused result of the two images. The wind input is from the east (right).

Table 2
Root mean square errors (RMSEs) of area-averaged velocity ratios between retrieved and actual urban geometry in different LES experiments (wind directions) and average sizes. The larger value in each row is in bold.

Wind direction	Average size	RMSEs real footprint	RMSEs extracted footprint
East	200 m × 200 m	**0.042**	0.038
East	100 m × 100 m	**0.046**	0.044
Southwest	200 m × 200 m	0.012	**0.022**
Southwest	100 m × 100 m	0.016	**0.029**

model. This is challenging because urban wind environments are extremely sensitive to urban morphologies and building geometries [5,39]. The accuracy requirement for urban geometries and building heights for AVA studies may be higher than that for other studies, such as thermal analysis without considering wind effects. As one can imagine, the effects of buildings on thermal conditions arise mainly through shading and anthropogenic heat generated by the buildings, and these effects are more localized than effects of building geometries on the wind environment.

Our results show that simulated pedestrian-level wind speed is sensitive to the given wind direction, which in essence is sensitive to building geometries. The term “roughness length” in PALM is not the city-scale roughness length that is applied in wind tunnel tests, but the so-called “local roughness length” that is imposed in each local grid box adjacent to a horizontal or vertical surface [30]. The city-scale roughness length in front of the targeted area (a city or neighborhood) for generating the input wind profile in wind tunnel tests or CFD is not involved in the LES experiments in this study. The reason is to save simulation domain, and in turn, computational time. As mentioned, a vertically unique wind velocity is imposed. Associated with the cyclic boundary condition setting and adequate time (4 h) for turbulence spin-up, a sufficient vertical wind profile can be generated in the simulation.

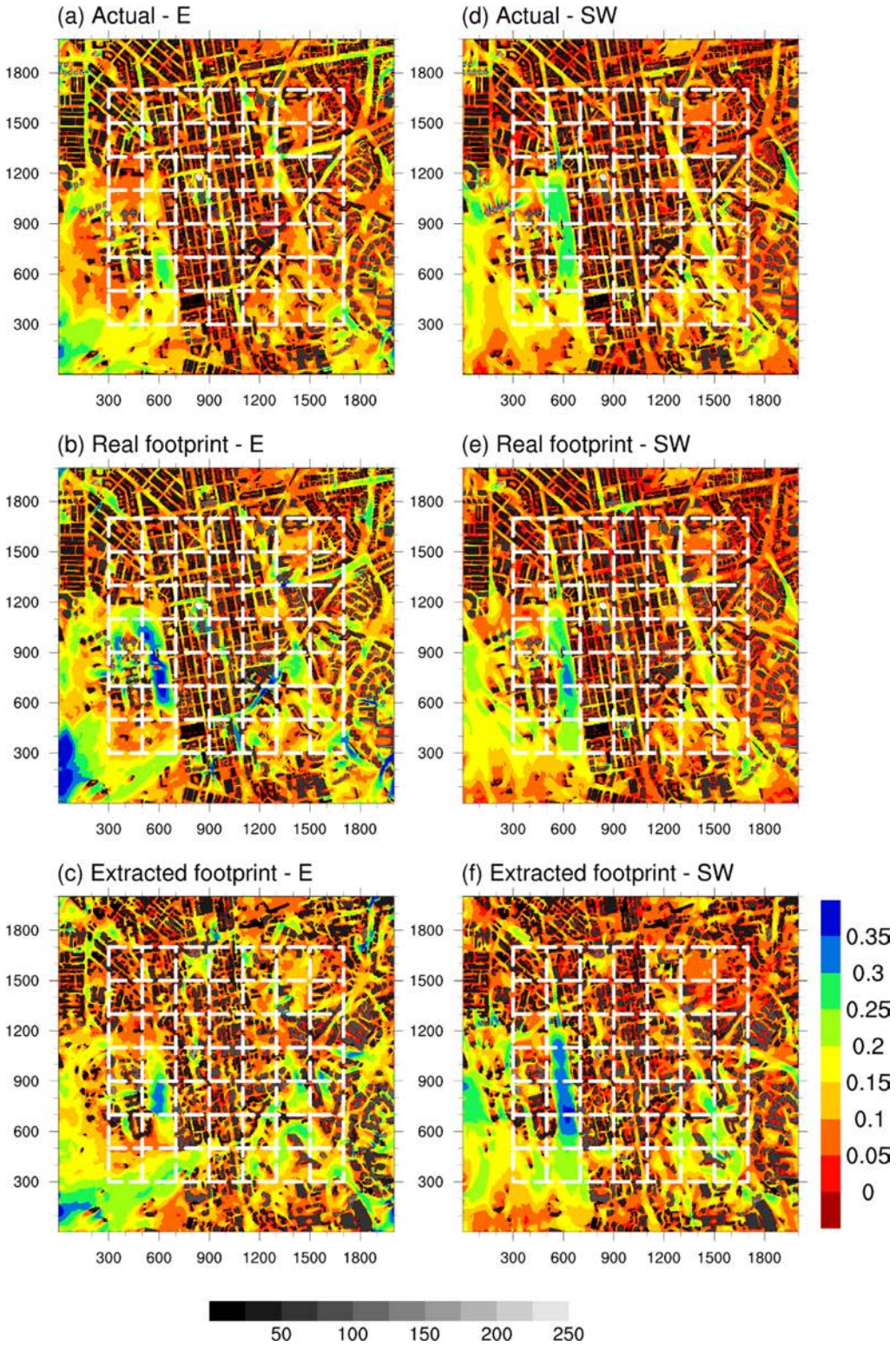

Fig. 12. PALM-computed velocity ratio in (a, d) actual topography, (b, e) fused building heights with real footprints, and (c, f) fused building heights with footprints extracted from stereo images. Wind input is from the east (southwest) in a–c (d–f). The dashed white boxes denote the 200 m × 200 m domains for the zonally averaged velocity ratio. The gray bar denotes building height (m).

Studies on urban wind environments using the LES technique require accurate urban morphologies and building geometries, i.e., precise urban elevation data. For the retrieved data used in the first step of this study, building footprints are assumed to be known before the building heights are extracted. Hence the street patterns are basically the same among all four sets of data evaluated in this study, and differences in pedestrian velocity ratios are caused mainly by building height and building volume differences. However, building footprints are probably not known, in the case of not knowing the realistic elevation data. Therefore, in the second step of this study, as an essential supplement, building height retrievals from fused results of stereo and SAR satellite

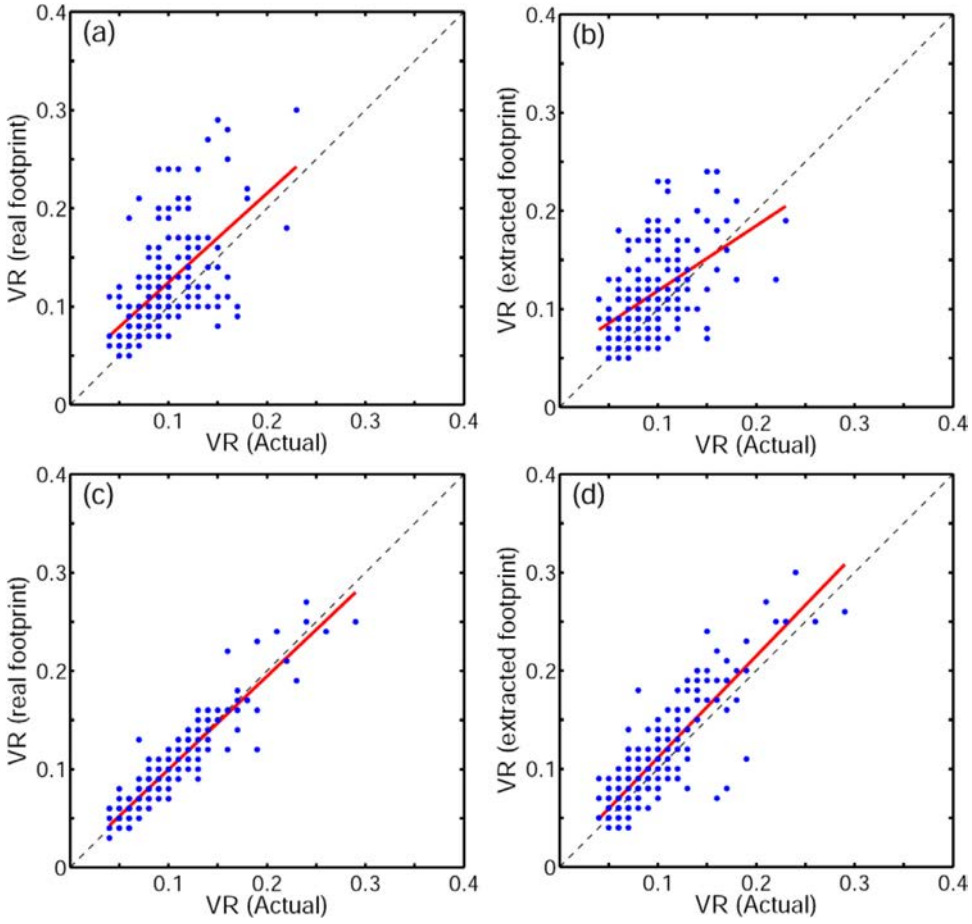

Fig. 13. Scatter plots (blue dots) and linear regressions (red solid lines) of PALM-computed velocity ratios with actual topography and topography fused results with (a, c) real footprints, and (b, e) footprints extract from stereo images. Wind input is from the east (southwest) for a–b (c–d). Average size is 100 m × 100 m. (For interpretation of the references to colour in this figure legend, the reader is referred to the web version of this article.)

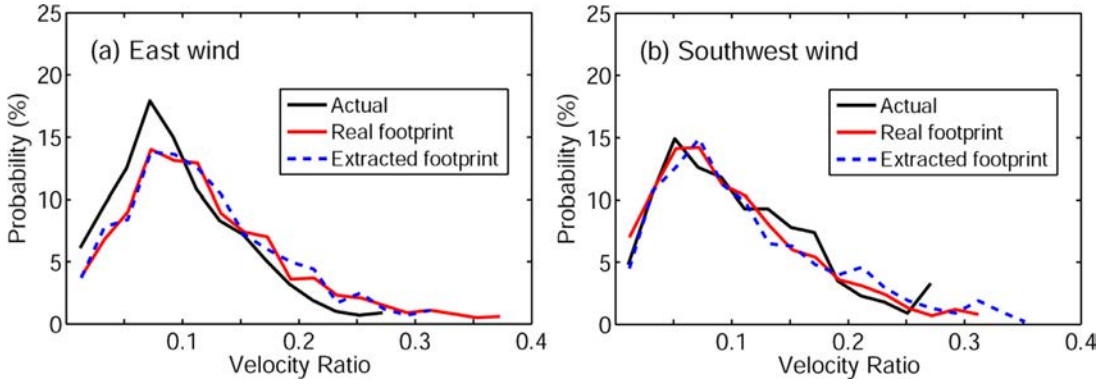

Fig. 14. Distributions of velocity ratios referenced at 2 m above the ground taken from random test points.

images with building footprints retrieved from stereo images are assessed by PALM-computed pedestrian-level ventilation. Finally, as an extension of the World Urban Database and Access (WUDAPT) (www.wudapt.org) method to provide two-dimensional urban form data for worldwide cities, the newly developed satellite-based method we evaluated in this study can quickly and efficiently produce accurate three-dimensional urban geometry data for cities where measured data of this kind are not accessible. This achievement can further support urban climate and air quality applications by urban planners and policy makers to mitigate and adapt to climate change through local actions.

7. Conclusions

This study performs a set of LES experiments using PALM to evaluate building geometry extraction from satellite images in an urban area of Mong Kok, Hong Kong. This comparative study is done from the practical perspective of urban ventilation. Major findings are summarized as follows: First, building heights extracted from stereo images have the worst performance compared to those from SAR images and the fused result of both images. Both the SAR and fused results can be considered acceptable for AVA purposes in this assessment in terms of their low RMSEs compared with the actual results. Second, it is known that high-rise

buildings produce strong concentrated wind loads at the pedestrian level, and it is documented that data extracted from stereo images produce better representations of low buildings, while data extracted from SAR images provide better results with high buildings. This may be the reason why a larger bias is found in the stereo results than in the SAR results with both east and southwest wind simulations. A further implication for this point is that retrieval methods with better representation of higher buildings, and in turn better reproduction of the overall urban-layer wind structure in CFD simulations, can obtain better urban ventilation results for AVA purposes. Third, both the area-averaged velocity ratios and velocity ratios taken from random test points indicate that the performance of building data retrieved from fused satellite images with and without actual building footprints is comparable, which implies that for pedestrian-level ventilation studies, building footprints extracted from stereo images are reliable. However, the performance of both sets of data in LES experiments is related to the input wind direction.

Some remaining issues for future work are: First, only two input wind directions, east for the annual prevailing wind and southwest for the summer prevailing wind, are simulated. To fully understand the impact of inflow direction on ventilation and assessment of building geometry extractions, more wind directions should be tested. Second, the current choice of grid spacing and model domain size is a tradeoff between limited computational power and high simulation accuracy. Hence, results from using a higher model resolution and larger model domain should be compared to the current results, in case stronger computational power is permitted. Third, all simulations in this study are based on a simple neutral assumption, without considering any thermal effects. Therefore, there is a need to take different kinds of atmospheric conditions beyond neutral, i.e., stable and unstable, into account in future work [40].

Acknowledgments

This study was supported by the Research Grants Council of the Hong Kong Special Administrative Region (Project No. 14408214), and Institute of Environment, Energy and Sustainability, CUHK (Project ID: 1907002).

References

[1] B. Blocken, W.D. Janssen, T. van Hooff, CFD simulation for pedestrian wind comfort and wind safety in urban areas: general decision framework and case study for the Eindhoven University campus, Environ. Modell. Softw. 30 (2012) 15–34.
[2] W. Wang, W. Zhou, E.Y.Y. Ng, Y. Xu, Urban heat islands in Hong Kong: statistical modeling and trend detection, Nat. Hazards 83 (2016) 885–907.
[3] A.J. Arnfield, Two decades urban research: a review of turbulence, exchanges of energy and water, and the urban heat island, Int. J. Climatol. 23 (2003) 1–26.
[4] E. Ng, Policies and technical guidelines for urban planning of high-density cities – air ventilation assessment (AVA) of Hong Kong, Build. Environ. 44 (2009) 1478–1488.
[5] X. Shi, Y. Zhu, J. Duan, R. Shao, J. Wang, Assessment of pedestrian wind environment in urban planning design, Landscape Urban Plann. 140 (2015) 17–28.
[6] E. Ng, V. Cheng, Urban human thermal comfort in hot and humid Hong Kong, Energy Build. 55 (2012) 51–65.
[7] R.E. Britter, S.R. Hanna, Flow and dispersion in urban areas, Annu. Rev. Fluid Mech. 35 (2003) 469–496.
[8] E. Ng, C. Yuan, L. Chen, C. Ren, J.C.H. Fung, Improving the wind environment in high-density cities by understanding urban morphology and surface roughness: a study in Hong Kong, Landscape Urban Plann. 101 (2011) 59–74.
[9] R. Ramponi, B. Blocken, L.B. de Coo, W.D. Janssen, CFD simulation of outdoor ventilation of generic urban configurations with different urban densities and equal and unequal street widths, Build. Environ. 92 (2015) 152–166.
[10] M. Skote, M. Sandberg, U. Westerberg, L. Claesson, A. Johansson, Numerical and experimental studies of wind environment in an urban morphology, Atmos. Environ. 39 (2005) 6147–6158.
[11] F. Yang, F. Qian, S.S.Y. Lau, Urban form and density as indicators for summertime outdoor ventilation potential: a case study on high-rise housing in Shanghai, Build. Environ. 70 (2013) 122–137.
[12] J. Unger, Intra-urban relationship between surface geometry and urban heat island: review and new approach, Climate Res. 27 (2004) 253–264.
[13] R. Emmanuel, E. Johansson, Influence of urban morphology and sea breeze on hot humid microclimate: the case of Colombo, Sri Lanka, Climate Res. 30 (2006) 189–200.
[14] F. Lindberg, C.S.B. Grimmond, Continuous sky view factor maps from high resolution urban digital elevation models, Climate Res. 42 (2010) 177–183.
[15] S. Eckert, T. Hollands, Comparison of automatic DSM generation modules by processing IKONOS stereo data of an urban area, IEEE J. Select. Top. Appl. Earth Observ. Remote Sens. 3 (2010) 162–167.
[16] E. Colin-Koeniguer, N. Trouve, Performance of building height estimation using high-resolution PolInSAR images, IEEE Trans. Geosci. Remote Sens. 52 (2014) 5870–5879.
[17] H. Sportouche, F. Tupin, L. Denise, Extraction and three-dimensional reconstruction of isolated buildings in urban scenes from high-resolution optical and SAR spaceborne images, IEEE Trans. Geosci. Remote Sens. 49 (2011) 3932–3946.
[18] G.Q. Zhou, X. Zhou, Seamless fusion of LiDAR and aerial imagery for building extraction, IEEE Trans. Geosci. Remote Sens. 52 (2014) 7393–7407.
[19] W. Rodi, J.H. Ferziger, M. Breuer, M. Pourquieé, Status of large eddy simulation: results of a workshop, J. Fluids Eng. 119 (1997) 248–262.
[20] T. Tamura, Towards practical use of LES in wind engineering, J. Wind Eng. Ind. Aerodyn. 96 (2008) 1451–1471.
[21] M.C. Castillo, A. Inagaki, M. Kanda, The effects of inner- and outer-layer turbulence in a convective boundary layer on the near-neutral inertial sublayer over an urban-like surface, Boundary Layer Meteorol. 140 (2011) 453–469.
[22] M. Keck, S. Raasch, M.O. Letzel, E. Ng, First results of high resolution large-eddy simulations of the atmospheric boundary layer, J. Heat Island Inst. Int. 9 (2014) 39–43.
[23] Y. Xu, P. Ma, E. Ng, H. Lin, Fusion of WorldView-2 stereo and Multitemporal TerraSAR-X images for building height extraction in urban areas, IEEE Geosci. Remote Sens. Lett. 12 (2015) 1795–1799.
[24] S. Raasch, M. Schröter, PALM - A large-eddy simulation model performing on massively parallel computers, Meteorol. Z. 10 (2001) 363–372.
[25] A. Inagaki, M.C.L. Castillo, Y. Yamashita, M. Kanda, H. Takimoto, Large-eddy simulation of coherent flow structures within a cubical canopy, Boundary Layer Meteorol. 142 (2011) 207–222.
[26] M. Kanda, A. Inagaki, T. Miyamoto, M. Gryschka, S. Raasch, A new aerodynamic parameterization for real urban surfaces, Boundary Layer Meteorol. 148 (2013) 357–377.
[27] S.-B. Park, J.-J. Baik, Large-eddy simulations of convective boundary layers over flat and urbanlike surfaces, J. Atmos. Sci. 71 (2014) 1880–1892.
[28] S.-B. Park, J.-J. Baik, S. Raasch, M.O. Letzel, A large-eddy simulation study of thermal effects on turbulent flow and dispersion in and above a street canyon, J. Appl. Meteorol. Climatol. 51 (2012) 829–841.
[29] A.A. Razak, A. Hagishima, N. Ikegaya, J. Tanimoto, Analysis of airflow over building arrays for assessment of urban wind environment, Build. Environ. 59 (2013) 56–65.
[30] M.O. Letzel, C. Helmke, E. Ng, X. An, A. Lai, S. Raasch, LES case study on pedestrian level ventilation in two neighbourhoods in Hong Kong, Meteorol. Z. 21 (2012) 575–589.
[31] B. Maronga, M. Gryschka, R. Heinze, F. Hoffmann, F. Kanani-Sühring, M. Keck, K. Ketelsen, M.O. Letzel, M. Sühring, S. Raasch, The Parallelized Large-Eddy Simulation Model (PALM) version 4.0 for atmospheric and oceanic flows: model formulation, recent developments, and future perspectives, Geosci. Model Dev. Discuss. 8 (2015) 1539–1637.
[32] Hong Kong Planning Department, Working Paper 2B: wind tunnel benchmarking studies, batch I, in: Urban Climatic Map and Standards for Wind Environment - Feasibility Study, 2008, p. 587.
[33] Y. Tominaga, A. Mochida, R. Yoshie, H. Kataoka, T. Nozu, M. Yoshikawa, T. Shirasawa, AIJ guidelines for practical applications of CFD to pedestrian wind environment around buildings, J. Wind Eng. Ind. Aerodyn. 96 (2008) 1749–1761.
[34] W. Wang, E. Ng, C. Yuan, S. Raasch, Large-eddy simulations of ventilation for thermal comfort — A parametric study of generic urban configurations with perpendicular approaching winds, Urban Clim. 20 (2017) 202–227.
[35] A. Mochida, Y. Tominaga, S. Murakam, R. Yoshie, T. Ishihara, R. Ooka, Comparison of various κ- ε models and DSM applied to flow around a high-rise building — Report on AIJ cooperative project for CFD prediction of wind environment, Wind Struct. 5 (2002) 227–244.
[36] H. Liu, Y. Jiang, B. Liang, F. Zhu, B. Zhang, J. Sang, Studies on wind environment around high buildings in urban areas, Sci. China Ser. D Earth Sci. 48 (2005) 102–115.
[37] S.H.L. Yim, J.C.H. Fung, A.K.H. Lau, S.C. Kot, Air ventilation impacts of the “wall effect” resulting from the alignment of high-rise buildings, Atmos. Environ. 43 (2009) 4982–4994.
[38] C. Ren, E. Ng, L. Katzschner, Urban climatic map studies: a review, Int. J. Climatol. 31 (2011) 2213–2233.
[39] P. Yang, G. Ren, W. Liu, Spatial and temporal characteristics of Beijing urban heat island intensity, J. Appl. Meteorol. Climatol. 52 (2013) 1803–1816.
[40] W. Wang, E. Ng, S. Raasch, H.L. Yim, C.K. Ho, Parametric studies of urban morphologies of high density cities and their air ventilation performance under neutral and unstable atmospheric conditions using advanced large-eddy simulations, in: The 9th International Conference on Urban Climate (ICUC), Toulouse, France, 2015, p. 6.